ACS Photonics

Letter

pubs.acs.org/journal/apchd5

Multifunctional Metamirror: Polarization Splitting and Focusing

Sergejs Boroviks,*[,†] Rucha A. Deshpande,[†] N. Asger Mortensen,[†,‡] and Sergey I. Bozhevolnyi*[,†,‡]

[†]Center for Nano Optics, University of Southern Denmark, Campusvej 55, DK-5230 Odense M, Denmark

[‡]Danish Institute for Advanced Study, University of Southern Denmark, Campusvej 55, DK-5230 Odense M, Denmark

ABSTRACT: Metasurfaces are paving the way to improve traditional optical components by integrating multiple functionalities into one optically flat metasurface design. We demonstrate the implementation of a multifunctional gap surface plasmon-based metasurface that in reflection mode splits orthogonal linear light polarizations and focuses them into different focal spots. The fabricated configuration consists of 50 nm thick gold nanobricks with different lateral dimensions organized in an array of 240 nm × 240 nm unit cells on top of a 50 nm thick silicon dioxide layer, which is deposited on an optically thick reflecting gold substrate. Our device features high efficiency (up to ∼65%) and polarization extinction ratio (up to ∼30 dB), exhibiting broadband response in the near-infrared band (750−950 nm wavelength) with the focal length dependent on the wavelength of the incident light. The proposed optical component can be forthrightly integrated into photonic circuits or fiber-optic devices.

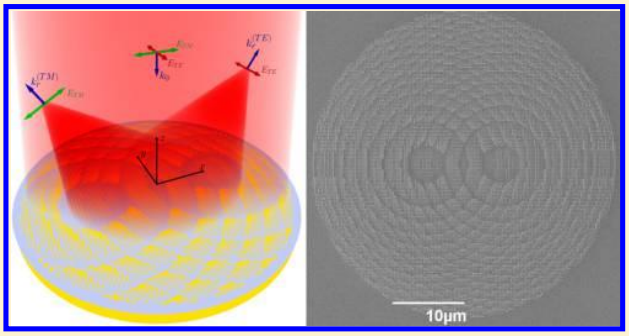

KEYWORDS: *gradient metasurfaces, flat optics, plasmonics, gap surface plasmons*

Optical metasurfaces[1−4]—planar (quasi-two-dimensional) subwavelength artificial metallic and dielectric structures—have developed tremendously in recent years.[5−11] With the progress in nanofabrication methods, different applications of metasurfaces have been demonstrated experimentally, ranging from artificial plasmonic coloring[12] to flat optical components.[13−17] In fact, many of the demonstrated functionalities cannot be realized with conventional (bulk) optical components (see recent reviews[18−20]). An important aspect of the development of flat optics is efficient integration of diverse functionalities into a single component of subwavelength thickness, which is also not attainable with conventional diffraction-limited optical components.[5] Thus, the scope of current research has recently been drawn to the exploration of *multifunctional* metasurfaces,[21−24] including reconfigurable designs.[25]

For polarization-controlled optical systems, for example, polarization-multiplexed fiber-optic communications[26] and polarization-assisted sensing,[27] single-chip multifunctionality is highly advantageous. Here we demonstrate the design of a multifunctional metasurface that can be straightforwardly used in such systems. It functions as a polarization-sensitive parabolic reflector (hereinafter called a polarization splitting and focusing metamirror (PSFMM)) that simultaneously splits orthogonal light polarizations and focuses them into different focal spots at the design wavelength, λ = 800 nm (an illustration of the working principle is shown in Figure 1). Previous designs targeted splitting of orthogonal polarizations in reflection and transmission and were implemented using dielectric or semiconductor metasurfaces[7,28,29] or alternatively in the radio frequency band.[30−32]

Our device utilizes gap surface plasmon (GSP) resonators[33−36] as constitutive elements, which support highly localized plasmonic resonances that form flexible meta-atom building blocks of metasurfaces,[1,2,18−20,37] with the possibility to engineer the local phase and reflection amplitude in gradient metasurfaces.[18,38] GSP-based metasurfaces operate in the reflection mode, which enables high efficiency,[15] reaching ∼80% for various applications.[39−41]

The basic element of the metasurface, also called the unit cell, has a period of Λ = 240 nm and comprises lithographically patterned gold nanobricks of height t = 50 nm and lateral dimensions L_x and L_y. The nanobricks are supported by a silicon dioxide layer (t_s = 50 nm) deposited on an optically thick gold substrate, as schematically depicted in the inset of Figure 2. Such a metal−insulator−metal (MIM) configuration is, in its nature, a GSP resonator that is known to exhibit strong field confinement in the dielectric layer under the metal nanobrick. Because of this property, negligible coupling between neighboring unit cells is permissibly assumed,[15] which facilitates the construction of phase-gradient metasurfaces.[18]

The electrodynamics of the considered MIM configuration was modeled using a finite-element method (Comsol Multiphysics), assuming that perpendicularly incident light (of wavelength λ = 800 nm) is polarized along the x axis.

Special Issue: Ultra-Capacity Metasurfaces with Low Dimension and High Efficiency

Received: September 19, 2017
Published: October 27, 2017

DOI: 10.1021/acsphotonics.7b01091
ACS Photonics 2018, 5, 1648−1653

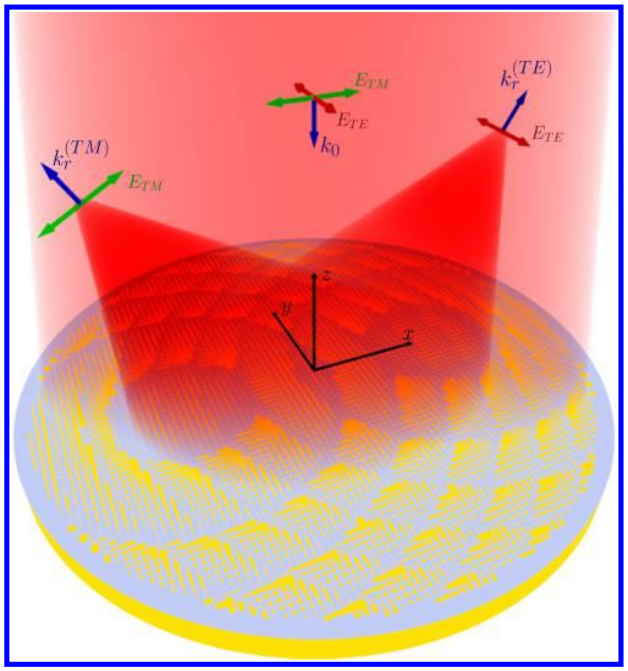

Figure 1. Illustration of the working principle (artistic rendering) of a multifunctional metasurface device. When illuminated by linearly polarized light, the device focuses and splits orthogonal linear light polarizations into different focal spots with high efficiency and a high polarization extinction ratio.

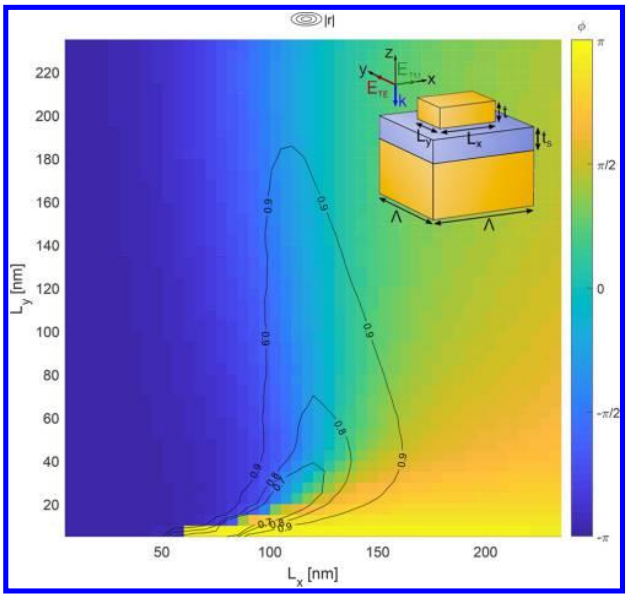

Figure 2. Simulated reflection coefficient $r = |r| \exp(i\phi)$, with the phase $\phi = \arg(r)$ shown by a color map as a function of the nanobrick lateral dimensions L_x and L_y for $\Lambda = 240$ nm and $t = t_s = 50$ nm for TM-polarized incident light at $\lambda = 800$ nm. Contour lines indicate the corresponding reflection coefficient amplitude $|r|$. The reflection phase and amplitude corresponding to TE polarization are obtained by transposing this map. (inset) Sketch of the metasurface unit cell with indicated dimensions.

Parametric sweeps were run through all possible combinations of nanobrick lateral dimensions L_x and L_y from 5 to 235 nm in steps of 5 nm, calculating the complex reflection coefficient, $r = |r| \exp(i\phi)$. The length of the step was chosen to comply with the resolution capability of the electron-beam lithography (EBL) used in our later fabrication of samples. Two degrees of freedom in the design geometry, i.e., the lateral dimensions of the gold nanobricks, give control over the reflection phase, ϕ, in almost full 2π phase space near the GSP resonance, as shown in the color map in Figure 2. Naturally, it is possible to control the phase response of the unit cell independently for two orthogonal linear light polarizations—transverse magnetic (TM) or x polarization, shown explicitly in Figure 2, and transverse electric (TE) or y polarization, which is equivalent to the transpose of the map shown in Figure 2. Except for a narrow region of dimensions close to the resonance, our generic GSP resonator facilitates a high reflection amplitude, $|r|$ (see the contour map in Figure 2), which is a crucial property for the overall efficiency of the metamirror.

DESIGN CONSIDERATIONS

In general, metasurfaces can be designed to mimic compact Fresnel reflectors by imposing a hyperboloidal phase profile on them.[42] The underpinning of this idea can be shown by investigating the optical path difference of rays reflected from the metasurface: as incident light is assumed to be a plane wave with a harmonic time dependence, $\mathbf{E}(\mathbf{x}, t) = \mathbf{E}_0 \exp[i(\mathbf{k}\cdot\mathbf{x} - \omega t)]$, the reflected rays differ from it only by a factor $\exp[i\phi_{(\alpha)}]$, which is the reflection phase (α indicates the polarization, i.e., either TM or TE). Phase accumulated in the redundant optical path can be compensated by letting the reflection phase on the metasurface follow a hyperboloidal profile, proportional to the incident wavenumber.

In our case, for simultaneous polarization splitting and focusing, two phase profiles are needed, one for each polarization, with centers of hyperboloids shifted one from another to achieve off-axis focusing. Thus, the reflection phase $\phi = \arg(r)$ in every cell of the metasurface must simultaneously satisfy two conditions:

$$\phi_{(\alpha)}(x, y) = \frac{2\pi}{\lambda}\left[d_z^{(\alpha)} - \sqrt{(x - d_x^{(\alpha)})^2 + (y - d_y^{(\alpha)})^2 + (d_z^{(\alpha)})^2}\right] \quad (1)$$

where $d_z^{(\mathrm{TM})}$ and $d_z^{(\mathrm{TE})}$, $d_x^{(\mathrm{TM})}$ and $d_x^{(\mathrm{TE})}$, and $d_y^{(\mathrm{TM})}$ and $d_y^{(\mathrm{TE})}$ are the coordinates of the focal points for TM and TE polarizations along the z, x, and y axes, respectively, as depicted in Figure 3a. A similar approach for achieving off-axis focusing has also been used in different contexts.[43,44]

In contrast to previous works,[13,15,42] we do not limit the choice of metasurface constitutive elements to some relatively small discrete design space. Instead, appropriate L_x and L_y parameters for each unit cell are chosen from the entire space of simulated values (Figure 2), namely, from the array of size 47× 47 elements. Even though it makes the optimization of our lithographic fabrication more complicated, the phase gradient obtained with this approach is closer to ideal, i.e., deviations from the imposed hyperboloidal phase profile introduced by fabrication imperfections are less pronounced compared with the case where the deviation is introduced also by relatively significant phase steps because of the limited number of constitutive elements, although the elements themselves are perhaps fabricated with better tolerances. One could also increase the variety of L_x and L_y parameters (e.g., by

DOI: 10.1021/acsphotonics.7b01091
ACS Photonics 2018, 5, 1648−1653

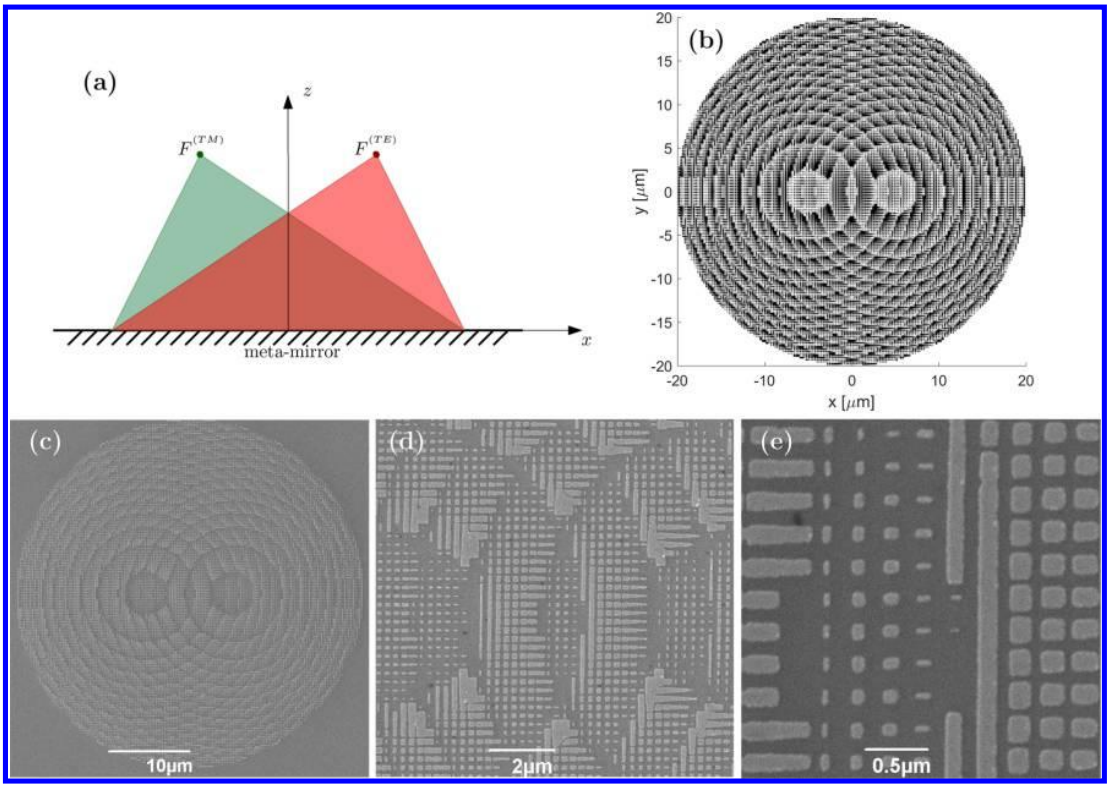

Figure 3. Design of the polarization splitting and focusing metamirror. (a) Locations of the focal points $F^{(\mathrm{TM})} = (d_x^{(\mathrm{TM})}, d_y^{(\mathrm{TM})}, d_z^{(\mathrm{TM})})$ and $F^{(\mathrm{TE})} = (d_x^{(\mathrm{TE})}, d_y^{(\mathrm{TE})}, d_z^{(\mathrm{TE})})$ for orthogonal linear light polarizations. (b) Geometry of the PSFMM design. (c–e) SEM images of the fabricated PSFMM sample at different magnifications with a zoom-in on the single-meta-atom building blocks of the metasurface.

interpolation within simulated values of L_x and L_y) to make the mapping to the ideal phase profile even more accurate. However, this would be an unnecessary complication since the discretization of the possible element dimensions is practically limited by the resolution of EBL equipment (~5 nm). Also, we do not impose any limitation on the minimal reflection amplitude of the constitutive elements, as elements with low $|r|$ for TM polarization have high values of the same parameter for TE (and vice versa), which on average results in reasonably good overall reflectivity and better correspondence to the imposed phase gradient.

The geometry of the PSFMM design selected for experimental investigation, with the focusing parameters set to $d_z^{(\mathrm{TM})} = d_z^{(\mathrm{TE})} = 15\ \mu$m, $d_x^{(\mathrm{TM})} = -d_x^{(\mathrm{TE})} = 5\ \mu$m, and $d_y^{(\mathrm{TM})} = d_y^{(\mathrm{TE})} = 0$, is shown in Figure 3b. This design diverges orthogonal polarizations by an angle of ~37° and focuses them at a distance of 15 μm from the metasurface. The metasurface design region is circular with diameter $D = 40\ \mu$m. The diameter defines the focusing ability of the metamirror, which is quantitatively measured in terms of the numerical aperture NA $\approx \sin[\tan^{-1}(D/2d_z^{(\alpha)})]$ (evaluated to be 0.8 for this design at the design wavelength, $\lambda = 800$ nm).

EXPERIMENTAL DETAILS

The multifunctional metamirror sample was fabricated using standard EBL and lift-off techniques. First, the substrate was prepared: a 150 nm-thick layer of Au and 50 nm of SiO_2, with a 3 nm-thin titanium layer in between for adhesion purposes, were deposited on a Si wafer using thermal evaporation (Cryofox TORNADO 405 evaporation system by Polyteknik) for the gold and titanium layers and radiofrequency sputtering for SiO_2. Furthermore, a 200 nm layer of PMMA 950 A2 resist (MicroChem), used as a stencil material for creating the nanobrick structures, was spin-coated. The PSFMM design pattern was then created using EBL (JEOL-640LV SEM with an ELPHY Quantum lithography attachment). The gold nanobricks were formed by thermal evaporation of 3 nm of Ti and 50 nm of Au followed by a lift-off process (etching away stencil material and development). As can be seen from scanning electron microscope (SEM) images in Figure 3c–e, apart from the smallest features, the fabrication quality of the resulting sample was in overall accordance with our initial design requirements also at the level of the meta-atom building blocks of the metasurface.

Optical characterization of the sample was performed using a tunable Ti-sapphire laser (3900S CW by Spectra-Physics), whose light was directed through a neutral density (ND) filter, a combination of a Glan–Thompson polarizer and a half-wave plate, and two beam splitters to a 60× objective (Edmund Optics, NA = 0.85, Achromatic, 0.15 mm working distance, chosen to have a higher NA than the designed metasurface), which was used to focus light onto the sample. The reflected light was collected using the same objective and directed via a beam splitter to an imaging lens, which focused light onto a CCD camera (Mightex CCEB013-U, monochrome), as schematically depicted in Figure 4a. Besides, additional white-light illumination was used for convenience of visually locating the metamirror on the surface of the sample. Since the fabricated multifunctional metamirror was designed to exhibit a very short focal distance (~15 μm), it was not practical to introduce a beam splitter between the sample surface and the

DOI: 10.1021/acsphotonics.7b01091
ACS Photonics 2018, 5, 1648–1653

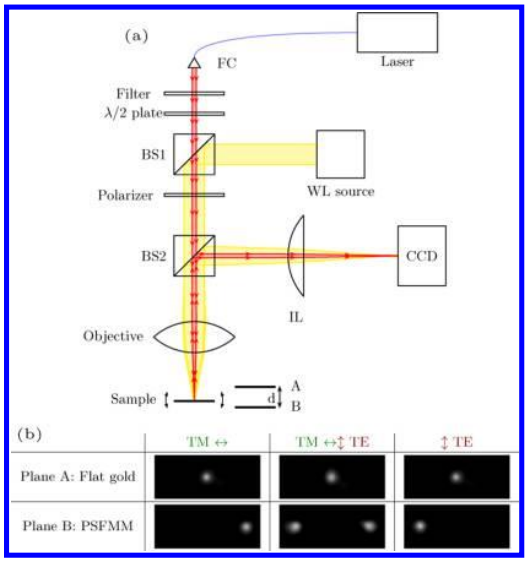

Figure 4. (a) Schematic diagram of the experimental setup for optical characterization of the fabricated sample. (b) Images of spots (brightness adjusted for better visibility) produced by the flat gold surface and PSFMM in planes A and B, respectively, upon illumination by the laser beam at λ = 800 nm with different polarizations.

objective to measure the focusing characteristics with an unfocused laser beam.

However, in this setup, the focusing effect could be verified by investigating how the fabricated metamirror and flat unstructured gold surface reflected light when placed at different distances from the objective. From geometrical optics, it can be shown that the plane at which the flat gold surface produces a focused spot on the CCD camera screen (denoted as plane A in Figure 4) is located at a distance $d = 2d_z^{(\alpha)}$ away from plane B, at which the PSFMM results in focused (deflected) spots on the screen.

Optical images of the spots created by the flat gold surface and multifunctional metamirror upon illumination of the sample with λ = 800 nm light in different polarization states are shown in Figure 4b. As can be seen, the PSFMM deflects TM polarization to the right-hand side and TE polarization to the left-hand side from the origin. Besides, raw images of the focal spots captured at different wavelengths were used to estimate the efficiency of the fabricated metamirror: the reflected power was determined by integrating the intensities of pixels in the captured images.

RESULTS AND DISCUSSION

The fabricated polarization-splitting and focusing metamirror sample was characterized and demonstrated comparatively good focusing characteristics at different wavelengths in the range of 750−950 nm, despite the inherent but minor imperfections in fabrication (Figure 3c−e). The measured focal length f (Figure 5a) is slightly smaller than its initially designed value (~13 μm instead of 15 μm at λ = 800 nm), but this deviation can be explained by the spherical aberration of the objective and imaging lens (we made no special effort to account for this). As was expected from the previous theoretical work,[13] the focal length of the metamirror decreases with increasing wavelength. It is worth noting that this chromatic aberration effect also decreases the NA value of the metamirror for longer wavelengths, as was also shown in a recent work on

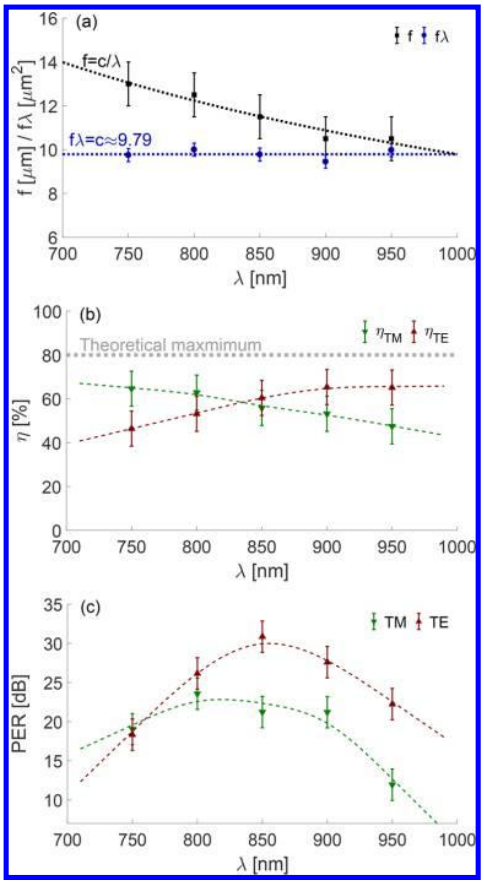

Figure 5. Performance of the fabricated PSFMM sample evaluated at five wavelengths in the 750−950 nm range. (a) Focal length f and $f\lambda$ product. The dotted lines emphasize the correspondence with idealized trends. (b) Efficiencies measured for orthogonal polarizations. The idealized theoretical maximum[13] is indicated by the gray dashed line. (c) Polarization extinction ratio, defined as the ratio of the intensities of the observed spots.

achromatic metasurfaces.[45] In turn, its $f\lambda$ product (a parameter that determines the dimensions of Fresnel zones for conventional Fresnel lenses and mirrors) is practically constant (~10 μm). This can be anticipated since there is no strong dispersion of the constitutive materials in the considered near-infrared wavelength range.

The efficiency, defined as the ratio of the powers of the light reflected by the metamirror located in plane B and by a flat unstructured gold surface in plane A, reached ~65% in the best case, which is significantly larger than in the previous demonstrations.[13,42] A previous numerical study of one-dimensional GSP-based focusing metamirrors[13] predicted the ultimate efficiency to be on the level of ~80% and also promised the broadband operation that we observed experimentally, with modest variations of properties across our wavelength regime of interest. The numerical simulations[13] did not suggest any clear trends in the wavelength dependences of key observables for relatively small wavelength variations. We thus attribute the observed spectral variations in our experiments mainly to unintended fabrication variations. In fact, taking the error bars into account, most of our observables are to a first approximation wavelength-independent, demonstrating high efficiency (>45%) over the entire measurement range.

DOI: 10.1021/acsphotonics.7b01091
ACS Photonics 2018, 5, 1648−1653

Finally, the polarization extinction ratio (PER) was studied (Figure 5c). Here the PER is defined as the ratio of the intensities of *correct* and *incorrect* spots upon illumination with a light of indicated polarization (shown on a dB scale). As can be seen, the PER is very high, reaching a value of 30 dB, which implies that only ∼1/1000 (conservative estimate) of the incident power is deflected into the incorrect focal spot. The error bars in Figure 5 indicate the measurement uncertainty due to inaccuracy in the axial positioning of the metamirror during the focal length measurement (±1 μm) and the unknown sensitivity of the CCD camera at different wavelengths (taken to be ±10% as a conservative estimate).

To summarize, we have demonstrated a broadband and efficient multifunctional metasurface that is capable of simultaneous focusing and polarization splitting. These functionalities capitalize on the highly in-plane-localized GSP modes hosted in an MIM configuration, which facilitate nearly independent reflection phase gradients for two orthogonal polarizations. Our class of devices can be directly integrated into various systems employing polarization multiplexing. While we have emphasized the near-infrared regime, the design can be readjusted to operate equally efficiently also in the telecommunication wavelength window. Finally, our EBL-based demonstration can be extended for large-scale fabrication, for example using roll-to-roll printing approaches now reaching out for metasurface mass production.[46,47]

AUTHOR INFORMATION

Corresponding Authors

*E-mail: sebo@mci.sdu.dk.
*E-mail: seib@mci.sdu.dk.

ORCID

Sergejs Boroviks: 0000-0002-3068-0284
N. Asger Mortensen: 0000-0001-7936-6264
Sergey I. Bozhevolnyi: 0000-0002-0393-4859

Notes

The authors declare no competing financial interest.

ACKNOWLEDGMENTS

S.I.B. acknowledges the European Research Council, Grant 341054 (PLAQNAP). N.A.M. is a VILLUM Investigator supported by VILLUM FONDEN (Grant 16498). The Center for Nano Optics is financially supported by the University of Southern Denmark (SDU 2020 funding). We acknowledge A. S. Roberts for help with fabrication issues, V. Zenin for suggestions on optical characterization, and J. Linnet for useful comments on an early version of the manuscript.

REFERENCES

(1) Kildishev, A. V.; Boltasseva, A.; Shalaev, V. M. Planar Photonics with Metasurfaces. *Science* **2013**, *339*, 1232009.
(2) Yu, N.; Capasso, F. Flat optics with designer metasurfaces. *Nat. Mater.* **2014**, *13*, 139−150.
(3) Zhao, Y.; Liu, X.-X.; Alù, A. Recent advances on optical metasurfaces. *J. Opt.* **2014**, *16*, 123001.
(4) Yu, N.; Capasso, F. Optical Metasurfaces and Prospect of Their Applications Including Fiber Optics. *J. Lightwave Technol.* **2015**, *33*, 2344−2358.
(5) Yu, N.; Genevet, P.; Kats, M. A.; Aieta, F.; Tetienne, J.-P.; Capasso, F.; Gaburro, Z. Light Propagation with Phase Discontinuities: Generalized Laws of Reflection and Refraction. *Science* **2011**, *334*, 333−337.
(6) Rogers, E. T. F.; Lindberg, J.; Roy, T.; Savo, S.; Chad, J. E.; Dennis, M. R.; Zheludev, N. I. A super-oscillatory lens optical microscope for subwavelength imaging. *Nat. Mater.* **2012**, *11*, 432−435.
(7) Arbabi, A.; Horie, Y.; Bagheri, M.; Faraon, A. Dielectric metasurfaces for complete control of phase and polarization with subwavelength spatial resolution and high transmission. *Nat. Nanotechnol.* **2015**, *10*, 937−943.
(8) High, A. A.; Devlin, R. C.; Dibos, A.; Polking, M.; Wild, D. S.; Perczel, J.; de Leon, N. P.; Lukin, M. D.; Park, H. Visible-frequency hyperbolic metasurface. *Nature* **2015**, *522*, 192−196.
(9) Lin, D.; Fan, P.; Hasman, E.; Brongersma, M. L. Dielectric gradient metasurface optical elements. *Science* **2014**, *345*, 298−302.
(10) Chong, K. E.; Staude, I.; James, A.; Dominguez, J.; Liu, S.; Campione, S.; Subramania, G. S.; Luk, T. S.; Decker, M.; Neshev, D. N.; Brener, I.; Kivshar, Y. S. Polarization-Independent Silicon Metadevices for Efficient Optical Wavefront Control. *Nano Lett.* **2015**, *15*, 5369−5374.
(11) Zhu, X.; Yan, W.; Levy, U.; Mortensen, N. A.; Kristensen, A. Resonant-laser-printing of structural colors on high-index dielectric metasurfaces. *Sci. Adv.* **2017**, *3*, e1602487.
(12) Kristensen, A.; Yang, J. K. W.; Bozhevolnyi, S. I.; Link, S.; Nordlander, P.; Halas, N. J.; Mortensen, N. A. Plasmonic colour generation. *Nat. Rev. Mater.* **2016**, *2*, 16088.
(13) Pors, A.; Nielsen, M. G.; Eriksen, R. L.; Bozhevolnyi, S. I. Broadband Focusing Flat Mirrors Based on Plasmonic Gradient Metasurfaces. *Nano Lett.* **2013**, *13*, 829−834.
(14) Pors, A.; Bozhevolnyi, S. I. Efficient and broadband quarter-wave plates by gap-plasmon resonators. *Opt. Express* **2013**, *21*, 2942−2952.
(15) Pors, A.; Albrektsen, O.; Radko, I. P.; Bozhevolnyi, S. I. Gap plasmon-based metasurfaces for total control of reflected light. *Sci. Rep.* **2013**, *3*, 2155.
(16) Ding, F.; Pors, A.; Chen, Y.; Zenin, V. A.; Bozhevolnyi, S. I. Beam-Size-Invariant Spectropolarimeters Using Gap-Plasmon Metasurfaces. *ACS Photonics* **2017**, *4*, 943−949.
(17) Wu, P. C.; Tsai, W.-Y.; Chen, W. T.; Huang, Y.-W.; Chen, T.-Y.; Chen, J.-W.; Liao, C. Y.; Chu, C. H.; Sun, G.; Tsai, D. P. Versatile Polarization Generation with an Aluminum Plasmonic Metasurface. *Nano Lett.* **2017**, *17*, 445−452.
(18) Ding, F.; Pors, A.; Bozhevolnyi, S. I. Gradient metasurfaces: a review of fundamentals and applications. *Rep. Prog. Phys.* **2017**, DOI: 10.1088/1361-6633/aa8732.
(19) Glybovski, S. B.; Tretyakov, S. A.; Belov, P. A.; Kivshar, Y. S.; Simovski, C. R. Metasurfaces: From microwaves to visible. *Phys. Rep.* **2016**, *634*, 1−72.
(20) Hsiao, H.-H.; Chu, C. H.; Tsai, D. P. Fundamentals and Applications of Metasurfaces. *Small Methods* **2017**, *1*, 1600064.
(21) Maguid, E.; Yulevich, I.; Veksler, D.; Kleiner, V.; Brongersma, M. L.; Hasman, E. Photonic spin-controlled multifunctional shared-aperture antenna array. *Science* **2016**, *352*, 1202−1206.
(22) Cheng, H.; Wei, X.; Yu, P.; Li, Z.; Liu, Z.; Li, J.; Chen, S.; Tian, J. Integrating polarization conversion and nearly perfect absorption with multifunctional metasurfaces. *Appl. Phys. Lett.* **2017**, *110*, 171903.
(23) Maguid, E.; Yulevich, I.; Yannai, M.; Kleiner, V.; L Brongersma, M.; Hasman, E. Multifunctional interleaved geometric-phase dielectric metasurfaces. *Light: Sci. Appl.* **2017**, *6*, e17027.
(24) Forouzmand, A.; Mosallaei, H. Real-Time Controllable and Multifunctional Metasurfaces Utilizing Indium Tin Oxide Materials: A Phased Array Perspective. *IEEE Trans. Nanotechnol.* **2017**, *16*, 296−306.
(25) Wu, P. C.; Zhu, W.; Shen, Z. X.; Chong, P. H. J.; Ser, W.; Tsai, D. P.; Liu, A.-Q. Broadband Wide-Angle Multifunctional Polarization Converter via Liquid-Metal-Based Metasurface. *Adv. Opt. Mater.* **2017**, *5*, 1600938.
(26) Core, M. T. Cross polarization interference cancellation for fiber optic systems. *J. Lightwave Technol.* **2006**, *24*, 305−312.

DOI: 10.1021/acsphotonics.7b01091
ACS Photonics 2018, 5, 1648−1653

(27) Caucheteur, C.; Guo, T.; Albert, J. Polarization-Assisted Fiber Bragg Grating Sensors: Tutorial and Review. *J. Lightwave Technol.* **2017**, *35*, 3311−3322.
(28) Guo, Z.; Zhu, L.; Shen, F.; Zhou, H.; Gao, R. Dielectric metasurface based high-efficiency polarization splitters. *RSC Adv.* **2017**, *7*, 9872−9879.
(29) Lee, J. H.; Yoon, J. W.; Jung, M. J.; Hong, J. K.; Song, S. H.; Magnusson, R. A semiconductor metasurface with multiple functionalities: A polarizing beam splitter with simultaneous focusing ability. *Appl. Phys. Lett.* **2014**, *104*, 233505.
(30) Cai, T.; Tang, S.; Wang, G.; Xu, H.; Sun, S.; He, Q.; Zhou, L. High-Performance Bifunctional Metasurfaces in Transmission and Reflection Geometries. *Adv. Opt. Mater.* **2017**, *5*, 1600506.
(31) Guo, W.; Wang, G.; Li, H.; Zhuang, Y.; Shuai, C. Ultra-thin reflecting polarization beam splitter under spherical waves' illumination by using single-layered anisotropic metasurface. *Appl. Phys. A: Mater. Sci. Process.* **2017**, *123*, 103.
(32) Xu, H.-X.; Tang, S.; Wang, G.-M.; Cai, T.; Huang, W.; He, Q.; Sun, S.; Zhou, L. Multifunctional Microstrip Array Combining a Linear Polarizer and Focusing Metasurface. *IEEE Trans. Antennas Propag.* **2016**, *64*, 3676−3682.
(33) Miyazaki, H. T.; Kurokawa, Y. Controlled plasmon resonance in closed metal/insulator/metal nanocavities. *Appl. Phys. Lett.* **2006**, *89*, 211126.
(34) Kurokawa, Y.; Miyazaki, H. T. Metal-insulator-metal plasmon nanocavities: Analysis of optical properties. *Phys. Rev. B: Condens. Matter Mater. Phys.* **2007**, *75*, 035411.
(35) Bozhevolnyi, S. I.; Søndergaard, T. General properties of slow-plasmon resonant nanostructures: nano-antennas and resonators. *Opt. Express* **2007**, *15*, 10869−77.
(36) Søndergaard, T.; Bozhevolnyi, S. I. Strip and gap plasmon polariton optical resonators. *Phys. Status Solidi B* **2008**, *245*, 9−19.
(37) Roberts, A. S.; Pors, A.; Albrektsen, O.; Bozhevolnyi, S. I. Subwavelength Plasmonic Color Printing Protected for Ambient Use. *Nano Lett.* **2014**, *14*, 783−787.
(38) Pors, A.; Bozhevolnyi, S. I. Plasmonic metasurfaces for efficient phase control in reflection. *Opt. Express* **2013**, *21*, 27438−27451.
(39) Sun, S.; Yang, K.-Y.; Wang, C.-M.; Juan, T.-K.; Chen, W. T.; Liao, C. Y.; He, Q.; Xiao, S.; Kung, W.-T.; Guo, G.-Y.; Zhou, L.; Tsai, D. P. High-Efficiency Broadband Anomalous Reflection by Gradient Meta-Surfaces. *Nano Lett.* **2012**, *12*, 6223−6229.
(40) Chen, W. T.; Yang, K.-Y.; Wang, C.-M.; Huang, Y.-W.; Sun, G.; Chiang, I.-D.; Liao, C. Y.; Hsu, W.-L.; Lin, H. T.; Sun, S.; Zhou, L.; Liu, A. Q.; Tsai, D. P. High-Efficiency Broadband Meta-Hologram with Polarization-Controlled Dual Images. *Nano Lett.* **2014**, *14*, 225−230.
(41) Zheng, G.; Mühlenbernd, H.; Kenney, M.; Li, G.; Zentgraf, T.; Zhang, S. Metasurface holograms reaching 80% efficiency. *Nat. Nanotechnol.* **2015**, *10*, 308.
(42) Aieta, F.; Genevet, P.; Kats, M. A.; Yu, N.; Blanchard, R.; Gaburro, Z.; Capasso, F. Aberration-Free Ultrathin Flat Lenses and Axicons at Telecom Wavelengths Based on Plasmonic Metasurfaces. *Nano Lett.* **2012**, *12*, 4932−4936.
(43) Deng, Z.-L.; Zhang, S.; Wang, G. P. Wide-angled off-axis achromatic metasurfaces for visible light. *Opt. Express* **2016**, *24*, 23118−23128.
(44) Chen, B. H.; Wu, P. C.; Su, V.-C.; Lai, Y.-C.; Chu, C. H.; Lee, I. C.; Chen, J.-W.; Chen, Y. H.; Lan, Y.-C.; Kuan, C.-H.; Tsai, D. P. GaN Metalens for Pixel-Level Full-Color Routing at Visible Light. *Nano Lett.* **2017**, *17*, 6345−6352.
(45) Wang, S.; Wu, P. C.; Su, V.-C.; Lai, Y.-C.; Chu, C. H.; Chen, J.-W.; Lu, S.-H.; Chen, J.; Xu, B.; Kuan, C.-H.; Li, T.; Zhu, S.; Tsai, D. P. Broadband achromatic optical metasurface devices. *Nat. Commun.* **2017**, *8*, 187.
(46) Højlund-Nielsen, E.; Clausen, J. S.; Mäkela, T.; Thamdrup, L. H.; Zalkovskij, M.; Nielsen, T.; Li Pira, N.; Ahopelto, J.; Mortensen, N. A.; Kristensen, A. Plasmonic Colors: Toward Mass Production of Metasurfaces. *Adv. Mater. Technol.* **2016**, *1*, 1600054.
(47) Murthy, S.; Pranov, H.; Feidenhans'l, N.; Madsen, J. S.; Hansen, P. E.; Pedersen, H. C.; Taboryski, R. J. J. Plasmonic color metasurfaces fabricated by a high speed roll-to-roll method. *Nanoscale* **2017**, *9*, 14280−14287.

DOI: 10.1021/acsphotonics.7b01091
ACS Photonics 2018, 5, 1648−1653